

ONE-LOOP ELECTROWEAK CORRECTIONS FOR POLARIZED MÖLLER SCATTERING AT DIFFERENT RENORMALIZATION SCHEMES AND CONDITIONS

*A. G. Aleksejevs¹, S. G. Barkanova², A. N. Ilyichev³,
Yu. G. Kolomensky⁴, V. A. Zykunov⁵*

¹Memorial University, Corner Brook, Canada

²Acadia University, Wolfville, Canada

³National Center of Particle and High-Energy Physics, Minsk

⁴University of California, Berkeley, USA

⁵Belarussian State University of Transport, Gomel, Belarus

Using two different approaches, we perform detailed calculations of the one-loop (Next-to-Leading Order (NLO)) electroweak radiative corrections to the parity violating $e^-e^- \rightarrow e^-e^-(\gamma)$ scattering asymmetry. The first approach, more classical, relies on calculations «by hand» with reasonable approximations, the second approach relies on program packages FeynArts, FormCalc, LoopTools, and FORM. The detailed numerical analysis of the various contributions is provided for a wide range of energies relevant for the ultra-precise 11 GeV MOLLER experiment planned at the JLab, as well as future experiments at the International Linear Collider (ILC). The numerical results obtained within the on-shell renormalization scheme using two different sets of renormalization conditions are in excellent agreement. We also calculate the total NLO correction in the Constrained Differential Renormalization (CDR) scheme. Analysis of the results, along with the increasing experimental precision, shows that it is feasible that the corrections at the Next-to-Next-to-Leading Order (NNLO) level may be important for the next generation of experiments.

PACS: 12.15.Lk; 13.88.+e; 25.30.Bf

INTRODUCTION

The Möller scattering measurements are not only one of the oldest and the best-established tools of modern physics, but also a clean, powerful probe of New Physics (NP) effects [1, 2]. More recently, the significant interest to this process from both theoretical and experimental communities has been reignited by two precision experiments: E-158 [3, 4] at SLAC, which made the first observation of parity violation in electron–electron scattering, and MOLLER experiment planned at JLab [5, 6]. Both are dedicated to measuring the Parity-Violating (PV) asymmetry in the $e^-e^- \rightarrow e^-e^-(\gamma)$ scattering at low energies. The MOLLER experiment aims to measure the PV asymmetry in the scattering of longitudinally

polarized electrons off unpolarized electrons with a combined statistical and systematic uncertainty of 36 parts per billion [5]. With the estimated systematic contribution of 1%, the measurement will still be statistics-limited, and further improvements in precision might be possible with additional running time. The measurement of the electron's weak charge Q_W^e with a 2.3% accuracy planned by MOLLER would yield the most precise single measurement of the weak mixing angle $\sin^2 \theta_W$, with a fractional accuracy of 0.1%, at an average momentum transfer $Q^2 = 0.0056 \text{ GeV}^2$. At this precision, MOLLER can shed light on the discrepancy between the hadronic and leptonic determinations of $\sin^2 \theta_W$ at the Z -boson pole. Furthermore, the difference between the values of $\sin^2 \theta_W$ determined at the Z -boson pole and at low Q^2 is sensitive to the NP effects at TeV scales.

Before physics of interest can be extracted from the experimental data, radiative effects must be carefully treated. MOLLER's stated precision goal is significantly more ambitious than that of its predecessor E-158, so very precise theoretical input for this measurement will be crucial. In spite of significant earlier theoretical effort dedicated to calculations of Electroweak Radiative Corrections (EWC) (see the early review papers [7] and [8], more recent [9] and [10], and numerous additional references in our paper [11]), we believe that a new level of accuracy is required for the next-generation, high-precision experiments. To match the expected experimental systematic uncertainty, it is desirable to keep the theoretical uncertainty due to the radiative corrections at or below the 0.1% level. Obviously, calculating large sets of one-loop Feynman diagrams by hand is a tedious task. Recently, program packages such as FeynArts [12], FormCalc [13], LoopTools [13] and FORM [14] have created the possibility of handling the substantial number of diagrams reasonably quickly, minimizing probability of human errors, and preventing the rapid error accumulation often unavoidable with purely numerical methods. One of the key features of the presented work is to compare, step by step, the complete one-loop set of EWC to the PV Möller scattering asymmetry calculated first by hand and then with FeynArts, FormCalc, and LoopTools as base languages using two different renormalization conditions.

FeynArts is a Mathematica package which provides the generation and visualization of Feynman diagrams and amplitudes involving Standard Model particles. FormCalc, a Mathematica package, reads diagrams generated with FeynArts and evaluates amplitudes with the help of the program FORM in the analytical form. FORM, a successor to SCHOONSCHIP [15], is a Symbolic Manipulation System, which is also essential for our computer algebra-based method, and is used by FormCalc as a core program. LoopTools provides the many-point tensor coefficient functions and is used to numerically evaluate scalar and tensor one-loop integrals. In FormCalc, it is possible for the regularization to be done either by dimensional reduction or by the usual dimensional regularization scheme. After that, one may implement one of the two Renormalization Schemes (RS), the

on-shell scheme or the Constrained Differential Renormalization (CDR) scheme. For calculations done at the one-loop level, the CDR scheme is equivalent to regularization done by dimensional reduction in the $\overline{\text{MS}}$ scheme with redefined scale $\log \overline{M}^2 = \log \mu^2 + 2$, where \overline{M} and μ are the renormalization scales in the CDR and in the dimensional regularization method, respectively [13].

A complete automatization would limit the range of applications, so these packages are not «black box»; they require considerable human input on many stages. We call our approach based on FeynArts, FormCalc, LoopTools, and FORM «semi-automated». On the other hand, these packages allow modifications to better suit specific projects. In [16], for example, we adopted FeynArts and FormCalc for the NLO calculations of the differential cross section in electron–nucleon scattering. In general, the results obtained with these packages can be presented in both analytical and numerical form. However, our equations for the EWC to the scattering asymmetry obtained with FeynArts and FormCalc are too lengthy and cumbersome, so we present only approximate equations obtained by hand. However, as we show in the numerical analysis section, the agreement between numerical results obtained with the two methods — «by hand» and semi-automatic — is excellent.

An additional way to ensure that our NLO EWC calculations are perfectly correct is the detailed comparison of results calculated with different renormalization conditions within the same scheme. Of course, the sum of all radiative corrections forming a full gauge-invariant set must be independent of the choice of renormalization conditions. Paper [17], for example, clearly demonstrated the cancellation of gauge dependencies in one-loop corrections from self-energies, tadpoles, vertex and box diagrams to physical amplitudes for four-fermion processes. However, the agreement between the results evaluated in different renormalization schemes can be guaranteed only if we take into account all orders of perturbation expansion, not just NLO. Since in this article we are only dealing with one-loop corrections, we do not expect the results produced in different schemes to be identical. In fact, the difference we see between the results obtained with the on-shell and CDR schemes indicates the need to consider higher-order corrections. A detailed discussion was given, for example, in [18]. The NNLO corrections will be our next task.

For now, we concentrate on achieving the best accuracy possible in one selected scheme and perform NLO calculations using two methods and two sets of renormalization conditions. For that, we choose the on-shell renormalization scheme with two different sets of renormalization conditions, the approach proposed by W. Hollik in [19] (see also [20]) and the approach suggested by A. Denner in [21]. For brevity, we will call Hollik’s renormalization conditions HRC; and Denner’s conditions, DRC. It is obvious that any renormalization scheme is required to meet physical conditions, although it is possible to vary

renormalization conditions for the sake of simplicity of the problem and still keep the final gauge-invariant results unchanged. As a result, contributions to the cross section coming from the different nongauge-invariant loop corrections (self-energies and vertex corrections) could vary greatly depending on the choice of renormalization conditions.

The first goal of this paper is to calculate the full set of one-loop EWC, both numerically with no simplifications using semi-automatic approach and «by hand», analytically in a compact asymptotic form [22–24], and compare the results. Our second goal is to present comparison and analysis of the various contributions to the cross-section asymmetry calculated within the HRC and DRC renormalization conditions. Our third aim is to calculate the total NLO corrections in the CDR scheme and estimate the importance of the NNLO corrections for such high-precision experiments as MOLLER.

The rest of the paper is organized as follows. In Sec. 1 we provide details of the basic notation, the lowest-order (Born or Leading Order (LO)) and NLO contributions to Möller scattering. The same section gives a short description of photon emission which is essential for removal of nonphysical parameters from regularized infrared divergent cross section. The details of the HRC and DRC renormalization conditions and a discussion of gauge invariance can be found in Sec. 2. Analysis of analytical and numerical results in the on-shell RS using HRC and DRC renormalization conditions is given in the beginning of Sec. 3. Later, in the same section, the CDR results are discussed. Section 4 includes the analysis of possible effects of an additional new-physics massive neutral boson on the observable asymmetry. Our conclusions and future plans are discussed in Conclusion.

1. DEFINITIONS AND FRAMEWORK

In the Standard Model, the Born cross section for Möller scattering with the longitudinally polarized electrons

$$e^-(k_1) + e^-(p_1) \rightarrow e^-(k_2) + e^-(p_2) \quad (1)$$

can be represented in the form

$$\sigma^0 = \frac{\pi\alpha^2}{s} \sum_{i,j=\gamma,Z} [\lambda_-^{i,j} (u^2 D^{it} D^{jt} + t^2 D^{iu} D^{ju}) + \lambda_+^{i,j} s^2 (D^{it} + D^{iu})(D^{jt} + D^{ju})], \quad (2)$$

where $\sigma \equiv d\sigma/d \cos \theta$, and θ is the scattering angle of the detected electron with momentum k_2 in the center-of-mass system of the initial electrons. The set of momenta of initial (k_1 and p_1) and final (k_2 and p_2) electrons (see Fig. 1)

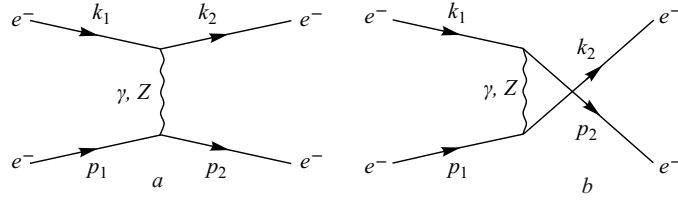


Fig. 1. Diagrams describing nonradiative Möller scattering in the t - (a) and u -channels (b)

generates the standard set of Mandelstam variables,

$$s = (k_1 + p_1)^2, \quad t = (k_1 - k_2)^2, \quad u = (k_2 - p_1)^2. \quad (3)$$

We neglect the electron mass m whenever possible and, in particular, when $m^2 \ll s, -t, -u$.

A useful structure we employ in this paper is

$$D^{ir} = \frac{1}{r - m_i^2} \quad (i = \gamma, Z; \quad r = t, u), \quad (4)$$

which depends on the Z -boson mass m_Z or on the photon mass $m_\gamma \equiv \lambda$. The photon mass is set to zero everywhere with the exception of specially indicated cases where the photon mass is taken to be an infinitesimal parameter that regularizes an infrared divergence. In addition, we use the functions

$$\lambda_{\pm}^{i,k} = \lambda_{1B}^{i,k} \lambda_{1T}^{i,k} \pm \lambda_{2B}^{i,k} \lambda_{2T}^{i,k}, \quad (5)$$

which are combinations of coupling constants and the degrees of polarizations $p_{B(T)}$ of the electrons with momentum k_1 (p_1) given by

$$\begin{aligned} \lambda_{1B(T)}^{i,j} &= \lambda_V^{i,j} - p_{B(T)} \lambda_A^{i,j}, & \lambda_{2B(T)}^{i,j} &= \lambda_A^{i,j} - p_{B(T)} \lambda_V^{i,j}, \\ \lambda_V^{i,j} &= v^i v^j + a^i a^j, & \lambda_A^{i,j} &= v^i a^j + a^i v^j. \end{aligned} \quad (6)$$

Here, vector and axial-vector parts of the couplings have the following structure:

$$\begin{aligned} v^\gamma &= 1, & a^\gamma &= 0, \\ v^Z &= \frac{I_e^3 + 2s_W^2}{2s_W c_W}, & a^Z &= \frac{I_e^3}{2s_W c_W}. \end{aligned} \quad (7)$$

It should be recalled that $I_e^3 = -1/2$ and $s_W(c_W)$ are the sine (cosine) of the Weinberg mixing angle which is defined in terms of m_Z and m_W according to the rules of the Standard Model (SM): $c_W = m_W/m_Z$ and $s_W = \sqrt{1 - c_W^2}$. The

electron degrees of polarization $p_{B(T)}$ are labeled such that the subscripts L and R correspond to the values of $p_{B(T)} = -1$ and $p_{B(T)} = +1$, respectively. Here, the first subscript indicates the degree of polarization for the momentum k_1 , while the second indicates the degree of polarization for the momentum p_1 . Combining the degrees of electron beam polarizations, we can obtain four measurable cross sections. However, by the virtue of the rotational invariance, two of them are identical: $\sigma_{LR} = \sigma_{RL}$. The three polarization cross sections can be used to construct three independent asymmetries [25]. Of particular interest to us is the parity-violating asymmetry A_{LR} which is defined as follows:

$$A_{LR} = \frac{\sigma_{LL} + \sigma_{LR} - \sigma_{RL} - \sigma_{RR}}{\sigma_{LL} + \sigma_{LR} + \sigma_{RL} + \sigma_{RR}} = \frac{\sigma_{LL} - \sigma_{RR}}{\sigma_{LL} + 2\sigma_{LR} + \sigma_{RR}}. \quad (8)$$

This single-polarization asymmetry corresponding to the scattering of longitudinally polarized electrons on unpolarized electrons is proportional to the combination $1 - 4s_W^2$, and is therefore highly sensitive to small changes in s_W . That is why the asymmetry A_{LR} was used as the observable in E-158 and will be measured in the future MOLLER experiment. At low energies and at Born level, the PV asymmetry A_{LR}^0 is given by

$$A_{LR}^0 = \frac{s}{2m_W^2} \frac{y(1-y)}{1+y^4+(1-y)^4} \frac{1-4s_W^2}{s_W^2}, \quad y = -\frac{t}{s}. \quad (9)$$

The contribution of virtual particles (V contribution) to the cross section of Möller scattering is described by the three classes of diagrams: boson self-energies (BSE) (they include $\gamma\gamma$, γZ , and ZZ self-energies and are shown symbolically in Fig. 2, *a*), vertex functions (Fig. 2, *b* and *c*), and two-boson exchange diagrams

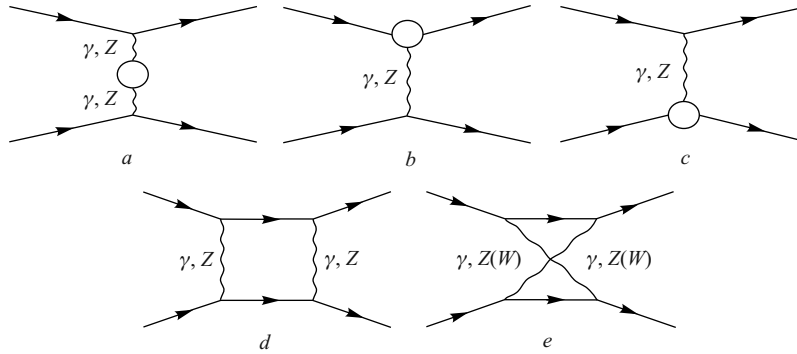


Fig. 2. One-loop t -channel diagrams for the Möller process. The circles represent the contributions of self-energies and vertex functions. The u -channel diagrams are obtained via the interchange $k_2 \leftrightarrow p_2$

(boxes) shown in Fig. 2, *d, e*. In the on-shell and CDR renormalization schemes there is no contribution from the electron self-energies. The corresponding cross section is given by the sum

$$\sigma^V = \sigma^{\text{BSE}} + \sigma^{\text{ver}} + \sigma^{\text{box}}. \quad (10)$$

The detailed expressions for all the terms in this sum were given in our recent paper [11].

Contributions coming from the vertex correction graphs (with a photon in the loop), as well as the $\gamma\gamma$ and γZ boxes suffer from the well-known infrared divergence. Regularization of this divergence can be done by giving the photon a small unphysical mass λ . Obviously, the final result should be free of unphysical parameters and hence such a dependence has to be removed. That can be done if we consider additional contributions associated with photon emission diagrams (bremsstrahlung). The detailed description of this contribution is also given in [11]. The bremsstrahlung cross section can be broken down into two parts (soft and hard) as

$$\sigma^R = \sigma_{\text{IR}}^R + \sigma_H^R \quad (11)$$

by separating the integration domain according to $k_0 < \omega$ and $k_0 > \omega$, where k_0 is the photon energy (in the reference frame co-moving with the center of mass of the primary electrons). The parameter ω corresponds to the maximum of the emitted soft-photon energy. First, we follow the methods of paper [26] to get a well-known result (see also [22–24, 27, 28]) for the soft-photon cross section (where e is the base of the natural logarithm):

$$\sigma_{\text{IR}}^R = \frac{\alpha}{\pi} \left(4 \log \frac{2\omega}{\lambda} \log \frac{tu}{em^2s} - \log^2 \frac{s}{em^2} + 1 - \frac{\pi^2}{3} + \log^2 \frac{u}{t} \right) \sigma^0. \quad (12)$$

Next, we sum the IR-terms of V and R contributions,

$$\begin{aligned} \sigma^C &= \sigma_{\text{IR}}^V + \sigma_{\text{IR}}^R = \\ &= \frac{\alpha}{\pi} \left(4 \log \frac{2\omega}{\sqrt{s}} \log \frac{tu}{em^2s} - \log^2 \frac{s}{em^2} + 1 - \frac{\pi^2}{3} + \log^2 \frac{u}{t} \right) \sigma^0 \end{aligned} \quad (13)$$

and get a result which is free of regularization parameter λ .

At this point, let us continue with the discussion of the details of renormalization conditions we use in our calculations.

2. RENORMALIZATION CONDITIONS AND GAUGE INVARIANCE

To obtain the ultraviolet-finite result and render the parameters of the Standard Model real, we have to apply a renormalization procedure. For a gauge-invariant set, physical results should be invariant under different renormalization conditions. That is, although the contributions of the different types of diagrams can

vary strongly for different renormalization conditions, the total impact of all one-loop virtual effects on observable quantities must remain independent. In other words, the contributions of separate self-energies and vertex correction functions strongly depend on the details of the renormalization conditions, and to properly account for the EWC, they should be taken as one gauge-independent set. We will illustrate this for the case of the observable A_{LR} , which is especially sensitive to the renormalization conditions. In addition, we can verify that our results are correct by comparing the computer-based (DRC) and «by hand» (HRC) calculations. We now briefly describe our two chosen renormalization conditions, DRC and HRC, within the on-shell renormalization scheme.

Both use multiplicative renormalization constants, and, as a result, the electroweak Lagrangian, originally written in terms of bare parameters, is separated into a basic Lagrangian and a counterterm Lagrangian. The basic Lagrangian has the same form as the bare one, but depends on renormalized parameters and fields. The counterterm Lagrangian depends on renormalization constants of masses, charges, and fields. Renormalization constants are fixed by the renormalization conditions, which are separated into two classes: the first determines the renormalization of the parameters, and the second fixes the renormalization of fields. The first class is related to physical observables at a given order of perturbation theory, and the second one is related to Green's functions and has no effect on calculations of S -matrix elements. Both approaches use essentially the same renormalization conditions to fix the parameters of the SM in the following way:

$$\begin{aligned} \text{Re } \hat{\Sigma}_T^W(m_W^2) = \text{Re } \hat{\Sigma}_T^{ZZ}(m_Z^2) = \text{Re } \hat{\Sigma}^f(m_f^2) = 0, \\ \hat{\Gamma}_\mu^{ee\gamma}(k^2 = 0, p^2 = m^2) = ie\gamma_\mu. \end{aligned} \quad (14)$$

Here, $\text{Re } \hat{\Sigma}_T^{ZZ,W}(m_{Z,W}^2)$ and $\hat{\Gamma}_\mu^{ee\gamma}(k^2 = 0, p^2 = m^2)$ are the real parts of the truncated, transverse renormalized boson self-energy and electron vertex correction graphs, respectively. The longitudinal parts of the boson self-energy make very small contributions and are not considered here. The first condition of Eq. (14) fixes the mass renormalization of the W , Z bosons and fermions without quark mixing. The second condition fixes the renormalization of electric charge, and is derived from the Thomson limit when momentum transfer $k^2 = 0$ and external electrons are on their mass shell. As for the renormalization conditions of the fields, both approaches are quite different. In HRC, field renormalization constants are determined from the following conditions:

$$\hat{\Sigma}_T^{\gamma Z}(0) = 0, \quad \frac{\partial}{\partial k^2} \hat{\Sigma}_T^\gamma(0) = 0. \quad (15)$$

However, in the DRC renormalization conditions, the field renormalization is defined on-shell, as it was done for renormalization of the SM parameters. This

explicitly introduces an additional set of conditions, besides Eq.(14) and (15), which read

$$\text{Re } \hat{\Sigma}_T^{\gamma Z}(m_Z^2) = 0, \quad \text{Re } \frac{\partial}{\partial k^2} \hat{\Sigma}_T^{ZZ}(m_Z^2) = 0, \quad \text{Re } \frac{\partial}{\partial k^2} \hat{\Sigma}_T^W(m_W^2) = 0. \quad (16)$$

As a result, in DRC, renormalization constants for the fields of vector bosons are calculated in a relatively simple way, without the mass-renormalization constants:

$$\begin{aligned} \delta Z_W^{(D)} &= -\text{Re} \frac{\partial}{\partial k^2} \Sigma_T^W(m_W^2), & \delta Z_Z^{(D)} &= -\text{Re} \frac{\partial}{\partial k^2} \Sigma_T^{ZZ}(m_Z^2), \\ \delta Z_{Z\gamma}^{(D)} &= \frac{2}{m_Z^2} \Sigma_T^{\gamma Z}(0), & \delta Z_{\gamma Z}^{(D)} &= -\frac{2}{m_Z^2} \text{Re} \Sigma_T^{\gamma Z}(m_Z^2), \\ \delta Z_{\gamma}^{(D)} &= -\frac{\partial}{\partial k^2} \Sigma_T^{\gamma}(0). \end{aligned} \quad (17)$$

They can be presented through truncated and nonrenormalized self-energy graphs. In comparison with HRC, where the renormalization conditions of Eq.(16) are not present, field renormalization constants are defined in a different way and depend on the mass renormalization constants:

$$\begin{aligned} \delta Z_{\gamma}^{(H)} &= -\frac{\partial}{\partial k^2} \Sigma_T^{\gamma}(0), \\ \delta Z_Z^{(H)} &= \frac{\partial}{\partial k^2} \Sigma_T^{\gamma}(0) - 2 \frac{c_W^2 - s_W^2}{s_W c_W} \frac{\Sigma_T^{\gamma Z}(0)}{m_Z^2} + 2 \frac{c_W^2 - s_W^2}{s_W^2} \left(\frac{\delta m_Z^2}{m_Z^2} - \frac{\delta m_W^2}{m_W^2} \right), \\ \delta Z_W^{(H)} &= \frac{\partial}{\partial k^2} \Sigma_T^{\gamma}(0) - 2 \frac{c_W}{s_W} \frac{\Sigma_T^{\gamma Z}(0)}{m_Z^2} + \frac{c_W^2}{s_W^2} \left(\frac{\delta m_Z^2}{m_Z^2} - \frac{\delta m_W^2}{m_W^2} \right), \\ \delta Z_{Z\gamma}^{(H)} &= \frac{c_W s_W}{c_W^2 - s_W^2} \left(\delta Z_Z^{(H)} - \delta Z_{\gamma}^{(H)} \right). \end{aligned} \quad (18)$$

The presence of the mass renormalization constants in the field-renormalization Eq.(18) increases the values of the truncated and renormalized self-energy diagrams, and the dominant NLO contributions to the observable cross section come from these diagrams. In DRC, the mass renormalization constants appear in renormalization constants of the electroweak couplings, and hence we observe comparable contributions coming from both self-energies and vertex corrections. Of course, such a comparison has no physical meaning since neither self-energies nor vertex corrections represent a gauge-invariant set on their own. As is well known, only the sum of both groups is gauge-invariant; later, we show that both approaches give exactly the same results for the observable asymmetry. We would like to highlight that it is important to exercise caution when comparing separate contributions arising from the different renormalization conditions. This

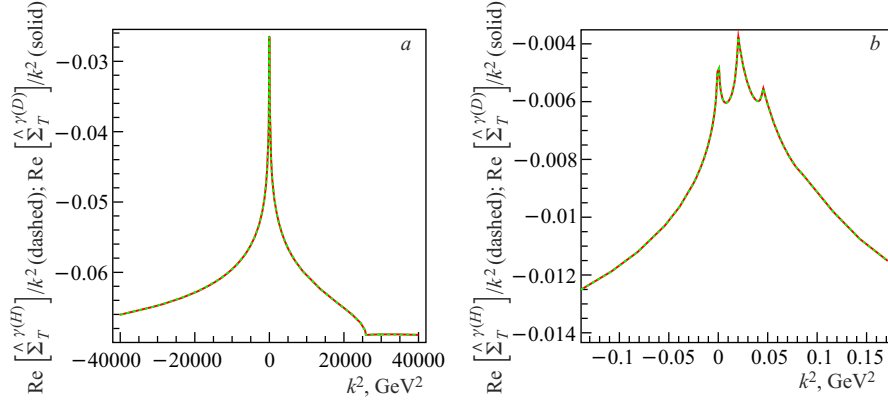


Fig. 3. Truncated and renormalized $\gamma\gamma$ self-energies in both sets of renormalization conditions. Plot *b* shows the low-energy domain

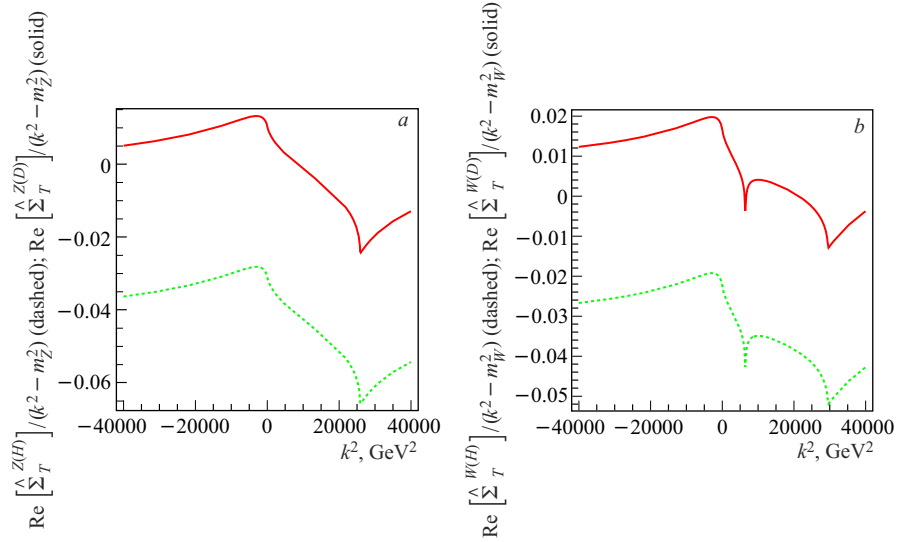


Fig. 4. Truncated and renormalized ZZ and WW self-energies in both sets of renormalization conditions

point is illustrated by Figs. 3, 4, and 5, where one can see various renormalized vector boson self-energies calculated with both DRC and HRC.

Let us note that the same renormalization conditions are imposed on the electromagnetic field. As we can see from Fig. 3, which shows the truncated

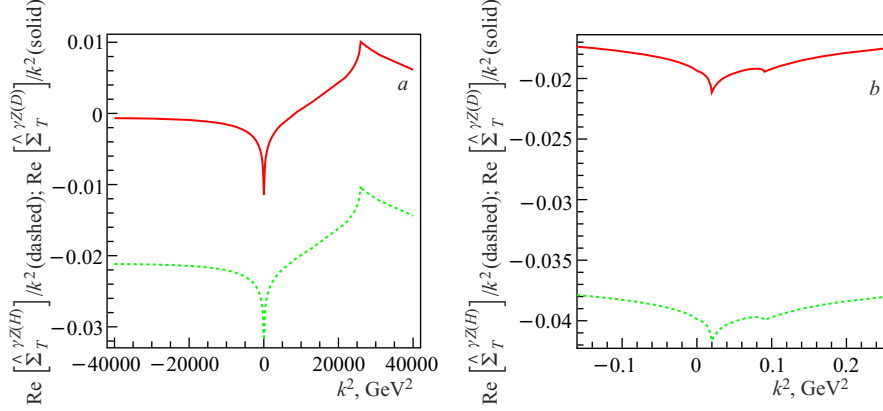


Fig. 5. Truncated and renormalized γZ self-energies in both sets of renormalization conditions. Plot *b* shows the low-energy domain

and renormalized $\gamma\gamma$ self-energies, there is no difference whatsoever between the two sets of conditions. The situation is quite different if we look at the results for the truncated and renormalized ZZ , γZ , and WW self-energies. In Figs. 4 and 5, we can see a substantial difference in the results obtained within the two sets of renormalization conditions, where the DRC set systematically leads to the self-energies being smaller in magnitude. As a result, with DRC, the self-energy contributions to Möller asymmetry are roughly a factor of two smaller in value compared to the values given by HRC. However, adding the DRC vertex corrections restores the total correction obtained with DRC to within 0.001% of the HRC result at all energies relevant to the planned MOLLER experiment at JLab.

Now we are ready to proceed to the analysis of the results. Subsubsection 3.1.1 is done in a manner independent of the renormalization conditions, and all notations that follow below can be applied to both DRC and HRC of the on-shell scheme.

3. RESULTS AND ANALYSIS

3.1. On-Shell Renormalization. For the numerical analysis, we use $\alpha = 1/137.035999$, $m_W = 80.399$ GeV, and $m_Z = 91.1876$ GeV according to [29], take electron, muon, and τ -lepton masses as $m_e = 0.510998910$ MeV, $m_\mu = 0.105658367$ GeV, $m_\tau = 1.77684$ GeV, and quark masses for loop contributions as $m_u = 0.06983$ GeV, $m_c = 1.2$ GeV, $m_t = 174$ GeV, $m_d = 0.06984$ GeV, $m_s = 0.15$ GeV, and $m_b = 4.6$ GeV. The light quark masses

provide $\Delta\alpha_{\text{had}}^{(5)}(m_Z^2) = 0.02757$ [30], where

$$\Delta\alpha_{\text{had}}^{(5)}(s) = \frac{\alpha}{\pi} \sum_{f=u,d,s,c,b} Q_f^2 \left(\log \frac{s}{m_f^2} - \frac{5}{3} \right), \quad (19)$$

Q_f is the electric charge of fermion f in proton charge units q ($q = \sqrt{4\pi\alpha}$). We can see that the use of the light quark masses as parameters regulated by the hadronic vacuum polarization is a better choice in this case. We checked that variations of the light quark masses around the outlined values have a negligible impact on the values of the polarization asymmetry, so the choice of quark masses does not introduce a significant uncertainty to our results. An earlier work by [9], relevant to observables measured at very low momentum transfers, which determined the weak mixing angle in the $\overline{\text{MS}}$ -scheme, also argued that the uncertainty from nonperturbative hadronic contributions is small compared to anticipated experimental uncertainties. Although [28] argued that the most significant source of theoretical uncertainty on scattering asymmetry comes from the hadronic contributions to the γZ vacuum polarization, we find that in our calculations hadronic contributions are under good control. Finally, for the mass of the Higgs boson, we take $m_H = 115$ GeV. A shift of the m_H value due to the recent CERN measurements of $m_H = 125\text{--}126$ GeV (which is still to be measured more exactly) does not change our results significantly.

Let us determine the physical impact of this contribution to the observable A_{LR} , by defining the relative corrections to the Born asymmetry as

$$\delta_A^C = \frac{A_{LR}^C - A_{LR}^0}{A_{LR}^0},$$

where the index C stands for a specific contribution, for example, $C = \text{BSE}$, ver , box . Let indices γSE , $\gamma Z\text{SE}$, and $Z\text{SE}$ denote $\gamma\gamma$ -, γZ -, and ZZ -BSE contributions, respectively. The main subject of the following analysis is «*weak*» relative corrections, which are defined as all BSE contributions (including the $\gamma\gamma$ -SE which is not weak by nature, but is needed here to account for all IR-finite contributions to the asymmetry) plus heavy vertex (HV) contributions («*heavy*» means «*massive*», i.e., Z or W boson), ZZ and WW boxes. In summary: $\text{weak} = \text{BSE} + \text{HV} + ZZ + WW$.

3.1.1. Analysis of BSE Contributions to PV Asymmetry. We start with the ZSE contribution, where

$$\delta_A^{\text{ZSE}} = \frac{A_{LR}^{\text{ZSE}} - A_{LR}^0}{A_{LR}^0} = \frac{(\sigma^0 + \sigma^{\text{ZSE}})|_{LL-RR} - \sigma^0|_{LL-RR}}{\sigma_{00}^0 + \sigma_{00}^{\text{ZSE}}} - \frac{\sigma^0|_{LL-RR}}{\sigma_{00}^0} \approx \frac{\sigma^{\text{ZSE}}|_{LL-RR}}{\sigma^0|_{LL-RR}}. \quad (20)$$

The operation $E|_{LL-RR}$ under expression E means $E_{LL} - E_{RR}$. Subscript 00 denotes the unpolarized cross section. The approximate equality is possible because $\sigma_{00}^{ZSE}/\sigma_{00}^0$ is very small. The denominator of the last fraction is calculated directly from Eq. (2):

$$\begin{aligned}\sigma^0|_{LL-RR} &= 16\pi\alpha^2 v^Z a^Z s (D^{\gamma t} + D^{\gamma u})(D^{Zt} + D^{Zu}) \approx \\ &\approx -32\pi\alpha^2 v^Z a^Z \frac{s}{m_Z^2} (D^{\gamma t} + D^{\gamma u}).\end{aligned}\quad (21)$$

With simplifications, the numerator of Eq. (20) is

$$\begin{aligned}\sigma^{ZSE}|_{LL-RR} &\approx \frac{\pi\alpha^2}{s} D_S^{ZZt} (D^{\gamma t} M_{\text{ev}}^{Z\gamma Z\gamma} - D^{\gamma u} M_{\text{od}}^{Z\gamma Z\gamma})|_{LL-RR} + (t \leftrightarrow u) \approx \\ &\approx -16\pi\alpha^2 v^Z a^Z \frac{s}{m_Z^4} (D^{\gamma t} + D^{\gamma u})(\hat{\Sigma}_T^Z(t) + \hat{\Sigma}_T^Z(u)).\end{aligned}\quad (22)$$

Finally,

$$\delta_A^{ZSE} \approx \frac{\hat{\Sigma}_T^Z(t) + \hat{\Sigma}_T^Z(u)}{2m_Z^2}.\quad (23)$$

At small r (Eq. (4)) corresponding to $E_{\text{lab}} = 11$ GeV and $\theta = 90^\circ$, the corrections are $\delta_A^{ZSE}(\text{HRC}) \approx 0.0309$ vs. $\delta_A^{ZSE}(\text{DRC}) \approx -0.0105$.

Similarly, for γZSE contribution

$$\begin{aligned}\sigma^{\gamma ZSE}|_{LL-RR} &\approx \frac{\pi\alpha^2}{s} D_S^{\gamma Zt} [D^{\gamma t} (M_{\text{ev}}^{\gamma\gamma Z\gamma} + M_{\text{ev}}^{Z\gamma\gamma\gamma}) - \\ &- D^{\gamma u} (M_{\text{od}}^{\gamma\gamma Z\gamma} + M_{\text{od}}^{Z\gamma\gamma\gamma})]|_{LL-RR} + (t \leftrightarrow u) \approx \\ &\approx 16\pi\alpha^2 a^Z \frac{s}{m_Z^2} (D^{\gamma t} + D^{\gamma u}) \left(\frac{\hat{\Sigma}_T^{\gamma Z}(t)}{t} + \frac{\hat{\Sigma}_T^{\gamma Z}(u)}{u} \right)\end{aligned}\quad (24)$$

and

$$\delta_A^{\gamma ZSE} \approx -\frac{1}{2v^Z} \left(\frac{\hat{\Sigma}_T^{\gamma Z}(t)}{t} + \frac{\hat{\Sigma}_T^{\gamma Z}(u)}{u} \right).\quad (25)$$

For γZSE at $E_{\text{lab}} = 11$ GeV and $\theta = 90^\circ$, the corrections are $\delta_A^{\gamma ZSE}(\text{HRC}) \approx -0.6028$ vs. $\delta_A^{\gamma ZSE}(\text{DRC}) \approx -0.2909$. It is important to note that the deviation in $\hat{\Sigma}_T^{\gamma Z}$ has a dramatic impact on such a sensitive observable as A_{LR} . For example, the uncertainty in $\hat{\Sigma}_T^{\gamma Z}$ of 1% will result in a change in $\delta_A^{\gamma ZSE}$ of up to 0.05.

All terms with properties of Eq. (20) contribute additively to the total correction, for example,

$$\delta_A^{\gamma ZSE+ZSE} \approx \delta_A^{\gamma ZSE} + \delta_A^{ZSE}.\quad (26)$$

We call such contributions *additive*. γSE gives a *nonadditive* and small contribution that we consider later.

3.1.2. *Analysis of HV and Box Contribution to PV Asymmetry.* Starting with the Λ_2 -contribution, which comes from the triangle diagrams with an additional massive boson, Z or W , we get

$$\delta_A^{\Lambda_2} \approx \frac{\sigma^{\Lambda_2}|_{LL-RR}}{\sigma^0|_{LL-RR}}. \quad (27)$$

The numerator, with some approximations, is

$$\sigma^{\Lambda_2}|_{LL-RR} \approx 8\alpha^3 v^Z a^Z s(D^{\gamma t} + D^{\gamma u}) \left(\frac{\Lambda_2(t, m_Z)}{t} + \frac{\Lambda_2(u, m_Z)}{u} \right), \quad (28)$$

so the correction is proportional to Λ_2 in the following way:

$$\delta_A^{\Lambda_2} \approx -\frac{\alpha m_Z^2}{4\pi} \left(\frac{\Lambda_2(t, m_Z)}{t} + \frac{\Lambda_2(u, m_Z)}{u} \right). \quad (29)$$

In HRC, we can simplify the result by using series expansion of Λ_2 at small t :

$$\Lambda_2(t, m_Z) = -\frac{t}{3m_Z^2} \left(2 \log \frac{-t}{m_Z^2} - \frac{23}{6} \right) + \mathcal{O} \left(\frac{t}{m_Z^2} \right), \quad (30)$$

which gives

$$\delta_A^{\Lambda_2} \approx \frac{\alpha}{6\pi} \left(\log \frac{tu}{m_Z^4} - \frac{23}{6} \right). \quad (31)$$

The numerical value obtained from above at $E_{\text{lab}} = 11$ GeV and $\theta = 90^\circ$ gives $\delta_A^{\Lambda_2} \approx -0.0125$, which is in agreement with the exact (semi-automatic) numerical calculations.

The Λ_3 -contribution, which represents the triangle diagrams with a 3-boson vertex, $WW\gamma$ or WWZ , is calculated in a similar way, so we present only the final result:

$$\delta_A^{\Lambda_3} \approx -\frac{3\alpha m_Z^2}{32\pi s_W^2 v^Z a^Z} \left(\frac{\Lambda_3(t, m_W)}{t} + \frac{\Lambda_3(u, m_W)}{u} \right). \quad (32)$$

After simplifications and series expansion of Λ_3 at small t ,

$$\Lambda_3(t, m_W) = -\frac{5t}{27m_W^2} + \mathcal{O} \left(\frac{t}{m_W^2} \right), \quad (33)$$

we find

$$\delta_A^{\Lambda_3} \approx \frac{\alpha}{\pi} \frac{5}{9(1-4s_W^2)}. \quad (34)$$

Using Eq. (34) for $E_{\text{lab}} = 11$ GeV and $\theta = 90^\circ$, we obtain $\delta_A^{\Lambda^3} \approx 0.0118$. Again, this approximate value calculated «by hand» is in very good agreement with the exact result obtained with our second, computer-based approach.

The box part is UV-finite and does not require the renormalization procedure. We divide the box contribution into QED ($\gamma\gamma$ and γZ boxes) and a heavy-box part (HB = $ZZ + WW$):

$$\sigma^{\text{box}} = \sigma_{\text{QED}}^{\text{box}} + \sigma_{\text{HB}}^{\text{box}}. \quad (35)$$

The types of boxes are shown in Fig. 2, *d*, *e*. The IR-divergent QED part of boxes (the first term in Eq. (35)) is described in detail both analytically and numerically in [11]. For the purely-weak part of the boxes (the second term), the equations are derived in the low-energy approximation.

The total *weak* correction to A_{LR} includes the HB cross section:

$$\sigma_{\text{HB}}^{\text{box}} = -\frac{\alpha^3}{s} \sum_{k=\gamma, Z} (B_{ZZ}^k + B_{WW}^k) + (t \leftrightarrow u), \quad (36)$$

where the expressions for B_{ij}^k take the form

$$\begin{aligned} B_{ZZ}^k &= D^{kt} \lambda_-^{Bk} \delta_{ZZ}^1 + (D^{kt} + D^{ku}) \lambda_+^{Bk} \delta_{ZZ}^2, \\ B_{WW}^k &= D^{kt} \lambda_-^{Ck} \delta_{WW}^1 + (D^{kt} + D^{ku}) \lambda_+^{Ck} \delta_{WW}^2. \end{aligned} \quad (37)$$

The combinations of the coupling constants are given in Eq. (5). Let us recall the coupling constants for the heavy boxes:

$$v^B = (v^Z)^2 + (a^Z)^2, \quad a^B = 2v^Z a^Z, \quad v^C = a^C = 1/(4s_W^2). \quad (38)$$

At $s, |t|, |u| \ll m_Z^2$, the corrections $\delta_{ij}^{1,2}$ have the form:

$$\begin{aligned} \delta_{ZZ}^1 &= \frac{3u^2}{2m_Z^2}, & \delta_{ZZ}^2 &= -\frac{3s^2}{2m_Z^2}, \\ \delta_{WW}^1 &= \frac{2u^2}{m_W^2}, & \delta_{WW}^2 &= \frac{s^2}{2m_W^2}. \end{aligned} \quad (39)$$

At last, after simplification at small t , for the relative corrections to PV asymmetry coming from heavy boxes we find:

$$\delta_A^{ZZ} \approx -\frac{3\alpha}{2\pi} v^B, \quad \delta_A^{WW} \approx \frac{\alpha}{4\pi s_W^2 (1 - 4s_W^2)}. \quad (40)$$

The numerical values obtained from the equations above at $E_{\text{lab}} = 11$ GeV and $\theta = 90^\circ$ give $\delta_A^{ZZ} \approx -0.0013$ and $\delta_A^{WW} \approx 0.0238$, which is once again in good agreement with the exact results evaluated with the help of the FeynArts, FormCalc, LoopTools and FORM program packages.

3.1.3. Numerical Analysis on EWC to PV Asymmetry. In the table below, we present the contributions to relative *weak* corrections calculated using two different approaches. In the first approach, we use approximate and compact expressions derived «by hand» with the application of HRC. In the second, we use computer-based analytical (FeynArts, FormCalc, and FORM) and numerical (LoopTools) calculations, with DRC.

The Born asymmetry A_{LR}^0 and the structure of relative *weak* corrections to it for $E_{\text{lab}} = 11$ GeV at different θ

Contributions	$\theta, ^\circ (A_{LR}^0, \text{ppb})$							
	20	30	40	50	60	70	80	90
	(6.63)	(15.19)	(27.45)	(43.05)	(60.69)	(77.68)	(90.28)	(94.97)
$\gamma\gamma$ -SE, DRC	-0.0043	-0.0049	-0.0054	-0.0058	-0.0062	-0.0064	-0.0066	-0.0067
$\gamma\gamma$ -SE, HRC	-0.0043	-0.0049	-0.0054	-0.0058	-0.0062	-0.0064	-0.0066	-0.0067
γZ -SE, DRC	-0.2919	-0.2916	-0.2914	-0.2912	-0.2911	-0.2910	-0.2909	-0.2909
γZ -SE, HRC	-0.6051	-0.6043	-0.6042	-0.6038	-0.6034	-0.6031	-0.6028	-0.6028
ZZ -SE, DRC	-0.0105	-0.0105	-0.0105	-0.0105	-0.0105	-0.0105	-0.0105	-0.0105
ZZ -SE, HRC	0.0309	0.0309	0.0309	0.0309	0.0309	0.0309	0.0309	0.0309
HV, DRC	-0.2946	-0.2633	-0.2727	-0.2703	-0.2714	-0.2712	-0.2711	-0.2710
HV, HRC	-0.0015	-0.0012	-0.0010	-0.0009	-0.0008	-0.0007	-0.0007	-0.0007
ZZ -box, exact	-0.0013	-0.0013	-0.0013	-0.0013	-0.0013	-0.0013	-0.0013	-0.0013
ZZ -box, approx.	-0.0013	-0.0013	-0.0013	-0.0013	-0.0013	-0.0013	-0.0013	-0.0013
WW -box, exact	0.0239	0.0238	0.0238	0.0239	0.0239	0.0238	0.0238	0.0238
WW -box, approx.	0.0238	0.0238	0.0238	0.0238	0.0238	0.0238	0.0238	0.0238
Total <i>weak</i> , DRC, exact	-0.5643	-0.5430	-0.5508	-0.5489	-0.5500	-0.5495	-0.5493	-0.5493
Total <i>weak</i> , HRC, approx.	-0.5526	-0.5514	-0.5511	-0.5505	-0.5500	-0.5496	-0.5493	-0.5493

The table demonstrates that the $\gamma\gamma$ -SE contribution is small, *nonadditive* and, as expected, is the same whether obtained in HRC or in DRC. The γZ -SE, ZZ -SE, and HV contributions are rather sizeable, are all additive, and are different for HRC and DRC. The ZZ -box contribution is small, and the WW -box one is dominant for the weak box correction. Both the ZZ box and WW box are additive and their sum is in excellent agreement regardless the method of calculations. The total relative *weak* correction is significant and in excellent agreement with the different methods. That confirms that we are dealing with a gauge-invariant set of graphs. The discrepancy between the two approaches is ~ 0.0001 at $\theta = 90^\circ$, but becomes larger with decreasing θ .

In Fig. 6, we can see the relative *weak* corrections shown by solid line for DRC (exact) and dotted line for HRC (approximate). The dashed line shows the QED correction obtained by including soft bremsstrahlung to the Born asymme-

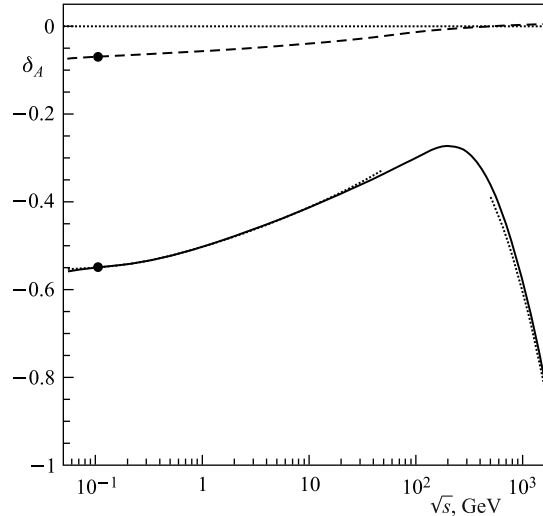


Fig. 6. The relative weak (solid line in DRC (semi-automated) and dotted line in HRC («by hand») and QED (dashed line) corrections to the Born asymmetry A_{LR}^0 versus \sqrt{s} at $\theta = 90^\circ$. The solid circle corresponds to our predictions for the MOLLER experiment

try A_{LR}^0 . We can see that for low-energy region $1 < \sqrt{s} < 30$ GeV, the results calculated by the two methods are in excellent agreement. It is worth mentioning here that the semi-automated numerical calculations of boxes in the region of $\sqrt{s} \ll 1$ GeV suffer from the numerical instability due to Landau singularities. As for our approximated calculations, we have used the small-energy approximation with the expansion parameters taken as $r/m_{Z,W}^2$ for energies $\sqrt{s} < 30$ GeV. In any case, for the 11 GeV relevant for the planned JLab experiment, the consistency of our calculations in both approaches is obvious, with a difference of $\sim 0.01\%$ or less. The dotted line for $\sqrt{s} > 500$ GeV in Fig. 6 is obtained using HRC with the help of equations from [31], which used the high-energy approximation. We can see good agreement between our results for the high-energy region $\sqrt{s} > 500$ GeV which becomes better with energy increase. For $\sqrt{s} \geq 50$ GeV we have excellent agreement with the result of [27] if we use their SM parameters (see [11]). Furthermore, the relative QED correction (see Fig. 8 in [27] and dashed line in Fig. 6 here) is also in good qualitative and numerical agreement. In this case, we apply the same cut on the soft photon emission energy as in [27] ($\omega/\sqrt{s} = 0.05$). At the low-energy point corresponding to the E-158 experiment, and using our set of input parameters (α , m_W , and m_Z), we find that $\delta_A^{\text{weak}} \approx -54\%$. If we translate our input parameters to the set α , G_F , and m_Z according to [27], we obtain good agreement with the result of [32].

3.2. Constrained Differential Renormalization. The CDR (Constrained Differential Renormalization) scheme, which provides renormalized expressions for Feynman graphs preserving the Ward identities, was introduced at the one-loop level in [33]. The [34] expands on [33] to introduce the techniques for one-loop calculations in any renormalizable theory in four dimensions. The procedure has been implemented in FormCalc and LoopTools, which allows us to evaluate NLO EWC in CDR. Since our «scheme of choice» at the moment is on-shell, which is more suitable for calculating EWC beyond one-loop, we do not provide the same detailed analysis and step-by-step comparison between the two methods for CDR as we do for on-shell. The reason we evaluate NLO EWC in CDR is to obtain some indication of the size of the higher-order effects (NNLO and beyond) to see if there is enough motivation to do these very involved calculations in the future.

In Fig. 7, we can see the relative total correction

$$\delta^{\text{tot}} = \frac{\sigma^{\text{tot}} - \sigma^0}{\sigma^0}$$

to the unpolarized cross section versus \sqrt{s} at $\theta = 90^\circ$ for different RS: on-shell and CDR. In the region of small energies, the difference between the two schemes is almost constant and rather small (~ 0.01), but grows at $\sqrt{s} \geq m_Z$. It is well known that in the region of small energies, the correction to the cross section is dominated by the QED contribution. However, in the high-energy region, the

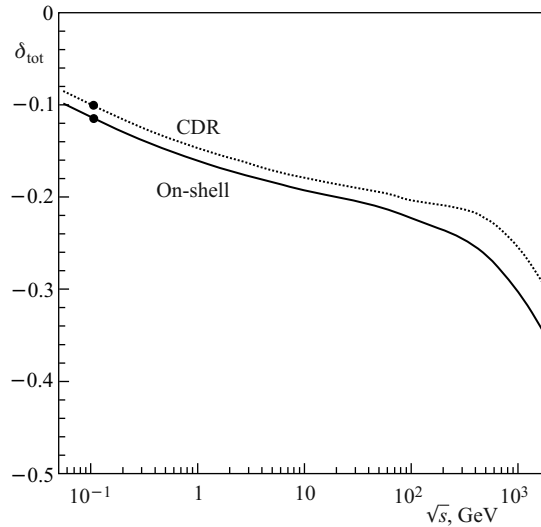


Fig. 7. The relative total corrections to the unpolarized cross section versus \sqrt{s} at $\theta = 90^\circ$. The filled circle corresponds to our predictions to the MOLLER experiment. Solid line corresponds to CDR; and dotted line, to on-shell RS

weak correction becomes comparable to QED. Since the difference between the on-shell and CDR results grows substantially as the weak correction becomes larger, it is clear that for an observable such as the PV asymmetry the difference between the on-shell and CDR schemes will be sizeable for the entire spectrum of energies $\sqrt{s} < 2000$ GeV. Because of that, we expect that the NNLO correction to the PV asymmetry may become important to PV precision physics in the future.

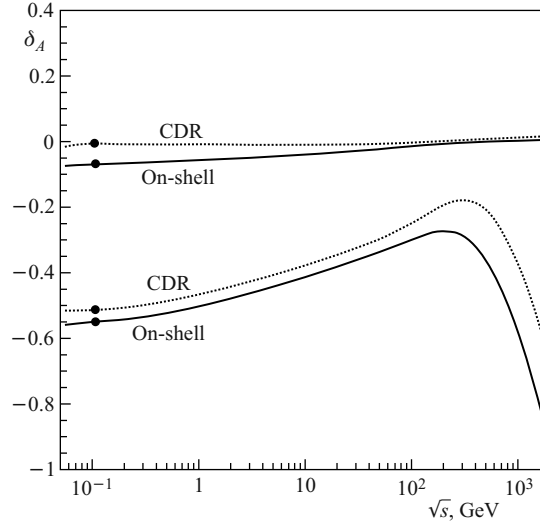


Fig. 8. The relative weak (lower lines) and QED (upper lines) corrections to the Born asymmetry A_{LR}^0 versus \sqrt{s} at $\theta = 90^\circ$. The filled circle corresponds to our predictions to the MOLLER experiment. Solid lines correspond to CDR; and dotted lines, to on-shell RS

Figure 8 shows the relative *weak* (lower lines), and QED (upper lines) corrections to the Born asymmetry A_{LR}^0 versus \sqrt{s} at $\theta = 90^\circ$. The difference is significant and is growing with increasing \sqrt{s} . According to our calculations for $E_{\text{lab}} = 11$ GeV, $\omega = 0.05\sqrt{s}$ and $\theta = 90^\circ$, the total radiative correction to PV asymmetry is -69.8% with on-shell and -58.5% with CDR. The difference is not at all surprising. For E-158, for example, the one-loop weak corrections were found to be about -40% in the $\overline{\text{MS}}$ scheme [32] and about -50% in the on-shell scheme [24,28].

The physical, NLO-corrected asymmetries, computed in both on-shell and CDR schemes, are compared in Fig.9. Here, for consistency with the $\overline{\text{MS}}$ definition of the couplings to $\mathcal{O}(\alpha)$ [35], we use $\hat{s}_Z^2 \equiv \sin^2 \hat{\theta}_W(M_Z) = 0.2313$ [29] in the expression of the Born asymmetry. We find that the predictions for the physical PV asymmetry, computed to the same order in perturbation theory in

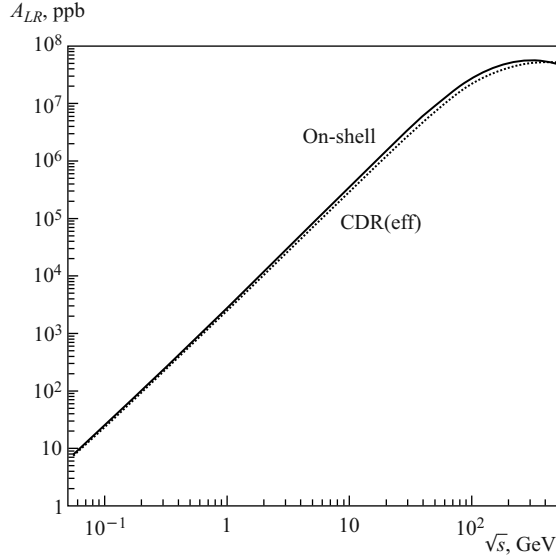


Fig. 9. The NLO-corrected asymmetries vs. \sqrt{s} at $\theta = 90^\circ$, computed in on-shell RS (solid line) and CDR (dotted line). The CDR Born asymmetry uses the $\overline{\text{MS}}$ definition of $\hat{s}_Z^2 \equiv \sin^2 \hat{\theta}_W(M_Z) = 0.2313$ [29]

two different schemes, differ by about 3%. The difference is an indication of the order of magnitude of the higher-order, NNLO and beyond, terms.

The [28] estimated that the higher-order corrections are suppressed by $\sim 0.1\%$ relative to the one-loop result, possibly 5% in some cases, and thus are not significant source of uncertainty. However, we conclude that although the corrections at the NNLO level were not mandated by the previously achievable experimental precision, they may become important for the next generation of experiments.

4. EFFECT OF ADDITIONAL MASSIVE NEUTRAL BOSON

Let us now add a very simple NP assumption to our SM calculations and show how this NP contribution affects the observable asymmetry. The reason we want to do it in here is to investigate if the two complimentary methods we used in the previous sections, «by-hand» and semiautomated, can be applied in the NP domain. As we mention in Introduction, FeynArts, FormCalc, LoopTools, and FORM are not «black box» programs and can be modified for specific projects, including adding the NP sector. As was already concluded in [36] and [37], the

proposed MOLLER measurement could be influenced by radiative loop effects of new-physics particles. This type of calculation is out of scope of this paper, but we plan to provide a full estimation in our future publication. For now, we assume that there is just one additional neutral boson (ANB), or Z' boson, with the usual $V - A$ structure of interaction with fermions, vector(axial) coupling constants $v^{Z'} (a^{Z'})$, and mass $m_{Z'}$. From the analysis done in the previous section, we can clearly see that in the low-energy region, where $s, |t|, |u| \ll m_Z^2 < m_{Z'}^2$, contributions are mainly suppressed by propagator factors like $D^{Z' r}$. In this section, our goal is to analyze the contribution of Z' -Born and ZZ' -box diagrams to the observable scattering asymmetry for the MOLLER experiment. The only significant contribution to the Born asymmetry comes from the interference terms from the Z' and photon diagrams. The relative correction to the Born asymmetry coming from Z' boson is additive, and is given by

$$\delta_A^{Z'} = \frac{v^{Z'} a^{Z'}}{v^Z a^Z} \frac{m_Z^2}{m_{Z'}^2}. \quad (41)$$

According to [5], the goal of MOLLER is to measure the PV asymmetry to a precision of 2% (0.73 ppb). With this uncertainty, and assuming the identical coupling constants for Z and Z' , it should be possible to detect ANB with a mass up to $m_{Z'} = \sqrt{m_Z^2/0.02} \approx 7m_Z$. The sensitivity of MOLLER to Z' increases if its parity-violating couplings are larger than those of Z^0 , making the measurements of PV complementary to the direct searches at high energies.

The one-loop diagrams including ANB give significantly smaller contributions. As an example, let us consider ZZ' box. As before, we perform our calculations by both approximate («by-hand») and exact (with FeynArts and FormCalc) methods, and get an excellent agreement. The expressions derived as a result of our approximate approach are presented below.

For the ZZ' -box contribution, the cross section can be expressed by the following short equation:

$$\sigma^{ZZ'\text{-box}} = \frac{3\alpha^3}{s} L \sum_{k=\gamma, Z} [\lambda_-^{B'k} (D^{kt} u^2 + D^{ku} t^2) - 2\lambda_+^{B'k} s^2 (D^{kt} + D^{ku})] + (Z \leftrightarrow Z'), \quad (42)$$

where

$$L = \int_0^1 z^2 dz \int_0^1 x dx \int_0^1 \frac{dy}{m_Z^2 z(x-1) + (t - m_{Z'}^2)(1-z)} \approx \frac{1}{m_Z^2 - m_{Z'}^2} \log \frac{m_{Z'}}{m_Z}, \quad (43)$$

and the functions $\lambda_{\pm}^{B'k}$ are expressed through

$$v^{B'} = v^Z v^{Z'} + a^Z a^{Z'}, \quad a^{B'} = v^Z a^{Z'} + v^{Z'} a^Z. \quad (44)$$

According to the methods described in Subsubsec. 3.1.1, we can now calculate the relative correction to the observable asymmetry from the ANB contribution (i.e., from ZZ' box) δ_A^{ANB} as

$$\delta_A^{\text{ANB}} = \frac{6\alpha m_Z^2}{\pi} \frac{v^{B'} a^{B'}}{v^Z a^Z} L. \quad (45)$$

This correction is additive and becomes less important with increasing $m_{Z'}$. However, this suppression is not very dramatic due to the growing log in the numerator. If we take the MOLLER kinematics and assume that $v^{Z'} = v^Z$, $a^{Z'} = a^Z$, then for $r_m \equiv m_{Z'}/m_Z = 1$ the correction is twice the contribution from ZZ box: $\delta_A^{\text{ANB}} \approx -0.0025465$. As r_m grows, the correction decreases: at $r_m = 2$ the correction is $\delta_A^{\text{ANB}} \approx -0.0011768$, and for $r_m = 10$ the correction is $\delta_A^{\text{ANB}} \approx -0.0001185$. At $r_m = 20$, the correction becomes completely negligible: $\delta_A^{\text{ANB}} \approx -0.0000382$. However, the possible contributions of new-physics particles to the Möller scattering deserves further attention, and we intend to continue our work in this direction.

One of the simplest supersymmetric SM extensions is the Minimal Supersymmetric Standard Model (MSSM), and it gives a useful framework for discussing SUSY phenomenology. For e^-e^- scattering, MSSM contributions will arise at the one-loop order, and the large suppression of the SM weak charge makes the weak charge sensitive to the effects of new physics. According to [36], the loop corrections in the MSSM can be as large as $\sim 4\%$ for the weak charge of the proton and $\sim 8\%$ for the weak charge of the electron, which is close to the current level of experimental and theoretical precision available for the low-energy studies. Obviously, before we can interpret these high-precision scattering experiments in terms of possible new physics, it is crucial to have the SM EWC under a very firm control.

CONCLUSION

In the presented work, we perform detailed calculations of the complete one-loop set of electroweak radiative corrections to the parity violating $e^-e^- \rightarrow e^-e^-(\gamma)$ scattering asymmetry both at low and high energies using the on-shell renormalization conditions proposed in [19] (see also [20]) and the conditions suggested in [21]. Although contributions from the self-energies and vertex diagrams calculated with the two sets of renormalization conditions differ significantly, our

full gauge-invariant set still guarantees that the total relative weak corrections are in excellent agreement for the two methods of calculation.

Obviously, it is important to exercise caution when comparing separate contributions arising from the different renormalization conditions unless these contributions form a gauge-invariant set (like boxes). Although this is a well-known fact, in principle, it is still useful to demonstrate this in detail numerically for a specific example. We hope that our results illustrating the structure of relative weak corrections evaluated at different renormalization conditions will be of educational value to researchers starting work in this area.

In addition, we compare the asymptotic results obtained analytically, «by hand» (with HRC), with some approximations, and semi-automatically (with DRC), with no approximations required. As a result, we have a good agreement for the whole $0 < \sqrt{s} < 50$ GeV energy region. More specifically, for the kinematics relevant to the 11 GeV MOLLER experiment planned at JLab, our agreement within two approaches for the complete one-loop set of electroweak radiative corrections is better than 0.1%. We found no significant theoretical uncertainty coming from the largest possible source, the hadronic contributions to the vacuum polarization. The dependence on other uncertain input parameters, like the mass of the Higgs boson, is extremely weak and well below 0.1%. We conclude that the excellent agreement we obtained between the results calculated «by hand» and semi-automatically serves as a good illustration of opportunities offered by FeynArts, FormCalc, LoopTools, and FORM.

Considering the large size of the obtained radiative effects, it is obvious that the careful procedure for taking into account radiative correction is essential. Our plans include the construction of a Monte Carlo generator for the simulation of radiative events within Möller scattering to make our work directly useful to the experiment. Since we are now assured of the reliability of our calculations, we plan to base this Monte Carlo on the maximum-precision results from our semi-automatic approach.

Although making sure that the results obtained by two different approaches using two renormalization conditions are identical assures us that our NLO EWC calculations are error-free, it does not address the question of the size of NNLO corrections. The two-loop corrections are beyond the scope of this work, but we plan to address them in the future. One way to find some indication of the size of higher-order contributions is to compare physical observables computed to the same order in perturbation theory in different renormalization schemes. Our calculations in the on-shell and CDR schemes show that while the NLO terms differ by about 11%, the PV asymmetries differ by about 3%. At the level of precision of the future experiments such as MOLLER, higher-order corrections become important.

To see if the two complementary approaches we successfully used for the SM calculations can be applied in the NP domain, we expanded FeynArts, FormCalc,

LoopTools, and FORM to include an additional neutral boson (Z'), calculated the relevant correction, and then obtained the same result by hand. Possible other contributions of new-physics particles to the Möller asymmetry still need to be investigated, and many of them can be included into the program packages mentioned above.

We believe that the future experiments at JLab and the ILC will mandate evaluation of the EWC beyond one loop. Once all the SM corrections are under control, it is worth considering NLO corrections including new-physics particles, starting with the Minimal Super Symmetric Model (MSSM). The most straightforward way to address these corrections is by employing the CDR scheme [33,34] because the CDR approach can be easily expanded to MSSM. However, whether the CDR scheme will be applicable in evaluating the EWC at the NNLO level is still an open question. Our preliminary plan is to address the NNLO EWC with the on-shell scheme first, and, if the effect is significant, stay with the same scheme for calculating contributions coming from the new-physics particles. The simple example of the ZZ' box we consider in Sec.4 is gauge-invariant and is thus not affected by the choice of renormalization, but we have to be careful when choosing the scheme for our future work. Any suggestions from the community regarding the best approach to this task would be greatly appreciated.

Acknowledgements. We are grateful to T. Hahn, K. Kumar, and E. Kuraev for stimulating discussions. A. A. and S. B. thank the Theory Center at JLab for hospitality in 2009 when this project was inspired. A. I. and V. Z. thank the Acadia and Memorial Universities for hospitality in 2010 and 2011. This work was supported by the Natural Sciences and Engineering Research Council of Canada and the Belarussian State Program of Scientific Researches «Convergence». V. Z. is grateful to A. Pavlenko and I. Prihod'ko for help in the framework of Program «Convergence».

REFERENCES

1. *Kumar K. S. et al.* Precision Low-Energy Weak Neutral Current Experiments // *Mod. Phys. Lett. A.* 1995. V. 10. P. 2979–2992.
2. *Kumar K. S.* The E158 Experiment // *Eur. Phys. J. A.* 2007. V. 32. P. 531–532.
3. *Anthony P. L. et al.* Observation of Parity Nonconservation in Möller Scattering // *Phys. Rev. Lett.* 2004. V. 92. P. 181602; hep-ex/0312035.
4. *Anthony P. L. et al.* Precision Measurement of the Weak Mixing Angle in Möller Scattering // *Phys. Rev. Lett.* 2005. V. 95. P. 081601; hep-ex/0504049.
5. *Benesch J. et al.* The MOLLER Collab. http://hallaweb.jlab.org/12GeV/Moller/downloads/DOE.Proposal/DOE_Moller.pdf. 2011.
6. *van Oers W. T. H. et al.* The MOLLER Experiment at Jefferson Lab: Search for Physics beyond the Standard Model // *AIP Conf. Proc.* 2010. V. 1261. P. 179–184.

7. *Mo L. W., Tsai Y. S.* Radiative Corrections to Elastic and Inelastic ep and μp Scattering // *Rev. Mod. Phys.* 1969. V. 41. P. 205–235.
8. *Maximon L. C.* Comments on Radiative Corrections // *Rev. Mod. Phys.* 1969. V. 41. P. 193–204.
9. *Erlter J., Ramsey-Musolf M. J.* The Weak Mixing Angle at Low Energies // *Phys. Rev. D.* 2005. V. 72. P. 073003; hep-ph/0409169.
10. *Kaiser N.* Radiative Corrections to Lepton–Lepton Scattering Revisited // *J. Phys. G.* 2010. V. 37. P. 115005.
11. *Aleksejevs A. et al.* Electroweak Radiative Corrections for Polarized Möller Scattering at Future 11 GeV JLab Experiment // *Phys. Rev. D.* 2010. V. 82. P. 093013; 1008.3355 [hep-ph].
12. *Hahn T.* Generating Feynman Diagrams and Amplitudes with FeynArts 3 // *Comp. Phys. Commun.* 2001. V. 140. P. 418–431; hep-ph/0012260v2.
13. *Hahn T., Perez-Victoria M.* Automatized One-Loop Calculations in Four Dimensions and D Dimensions // *Comp. Phys. Commun.* 1999. V. 118. P. 153–165.
14. *Vermaseren J.* New Features of FORM. 2000; math-ph/0010025.
15. *Strubbe H.* Manual for Schoonschip: A CDC 6000 / 7000 Program for Symbolic Evaluation of Algebraic Expressions // *Comp. Phys. Commun.* 1974. V. 8. P. 1–30.
16. *Aleksejevs A., Barkanova S., Blunder P. G.* Computational Model for Electron–Nucleon Scattering and Weak Charge of the Nucleon // *J. Phys. G.* 2009. V. 36. P. 045101.
17. *Degrassi G., Sirlin A.* Gauge Dependence of Basic Electroweak Corrections of the Standard Model // *Nucl. Phys. B.* 1992. V. 383. P. 73–92.
18. *Hollik W., Timme H.-J.* Renormalization Scheme Dependence of Electroweak Radiative Corrections // *Z. Phys. C.* 1986. V. 33. P. 125–133.
19. *Hollik W.* Radiative Corrections in the Standard Model and Their Role for Precision Tests of the Electroweak Theory // *Fortschr. Phys.* 1990. V. 38. P. 165–260.
20. *Böhm M., Spiesberger H., Hollik W.* On the One-Loop Renormalization of the Electroweak Standard Model and Its Application to Leptonic Processes // *Fortschr. Phys.* 1986. V. 34. P. 687–751.
21. *Denner A.* Techniques for Calculation of Electroweak Radiative Corrections at the One-Loop Level and Results for W Physics at LEP-200 // *Fortschr. Phys.* 1993. V. 41. P. 307–420.
22. *Zygunov V. A.* Electroweak Radiative Effects in the Möller Scattering of Polarized Particles // *Yad. Fiz.* 2004. V. 67. P. 1366–1379 (*Phys. At. Nucl.* 2004. V. 67. P. 1342–1354).
23. *Kolomensky Yu. G. et al.* Electroweak Radiative Corrections to Parity-Violating Asymmetry in Möller Scattering // *Intern. J. Modern Phys. A.* 2005. V. 20. P. 7365–7374.
24. *Zygunov V. A. et al.* First Order QED Corrections to the Parity-Violating Asymmetry in Möller Scattering. Preprint SLAC-PUB-11378. 2005; hep-ph/0507287v1.

25. *Cuypers F., Gambino P.* Polarization and Weak Mixing Angle in High-Energy e^+e^- Collisions // *Phys. Lett. B.* 1996. V. 388. P. 211–218.
26. *'t Hooft G., Veltman M.* Scalar One-Loop Integrals // *Nucl. Phys. B.* 1979. V. 153. P. 365–401.
27. *Denner A., Pozzorini S.* Electroweak Radiative Corrections to Polarized Möller Scattering at High Energies // *Eur. Phys. J. C.* 1999. V. 7. P. 185–195.
28. *Petriello F. J.* Radiative Corrections to Fixed Target Möller Scattering Including Hard Bremsstrahlung Effects // *Phys. Rev. D.* 2003. V. 67. P. 033006; hep-ph/0210259.
29. *Nakamura K. et al.* Review of Particle Physics // *J. Phys. G.* 2010. V. 37. P. 075021.
30. *Jegerlehner F.* Hadronic Contributions to the Photon Vacuum Polarization and Their Role in Precision Physics // *J. Phys. G.* 2003. V. 29. P. 101–110; hep-ph/0104304.
31. *Zykinov V. A.* Complete Calculation of Electroweak Corrections for Polarized Möller Scattering at High Energies // *Yad. Fiz.* 2009. V. 72. P. 1540–1554 (*Phys. At. Nucl.* 2009. V. 72. P. 1486–1500).
32. *Czarnecki A., Marciano W.* Electroweak Radiative Corrections to Polarized Möller Scattering Asymmetries // *Phys. Rev. D.* 1996. V. 53. P. 1066–1072.
33. *del Aguila F. et al.* Constraining Differential Renormalization in Abelian Gauge Theories // *Phys. Lett. B.* 1998. V. 419. P. 263–271.
34. *del Aguila F. et al.* Techniques for One-Loop Calculations in Constrained Differential Renormalization // *Nucl. Phys. B.* 1998. V. 537. P. 561–585; hep-ph/9806451v1.
35. *Sirlin A.* Role of $\sin^2\theta_W(m_Z)$ at the Z^0 Peak // *Phys. Lett. B.* 1989. V. 232. P. 123–126.
36. *Kurylov A., Ramsey-Musolf M. J., Su S.* Probing Supersymmetry with Parity Violating Electron Scattering // *Phys. Rev. D.* 2003. V. 68. P. 035008; hep-ph/0303026.
37. *Ramsey-Musolf M. J., Su S.* Low-Energy Precision Test of Supersymmetry // *Phys. Rep.* 2008. V. 456. P. 1–88; hep-ph/0612057.